Journal Pre-proof

Photoelectron imaging spectroscopic signatures of CO activation by the heterotrinuclear titanium-nickel clusters

Jianpeng Yang , Jumei Zhang , Shihu Du , Gang Li , Jinghan Zou , Qiangshan Jing , Hua Xie , Ling Jiang

PII: S1001-8417(22)00709-4
DOI: https://doi.org/10.1016/j.cclet.2022.07.045
Reference: CCLET 7702

To appear in: *Chinese Chemical Letters*

Received date: 17 June 2022
Revised date: 11 July 2022
Accepted date: 21 July 2022

Please cite this article as: Jianpeng Yang , Jumei Zhang , Shihu Du , Gang Li , Jinghan Zou , Qiangshan Jing , Hua Xie , Ling Jiang , Photoelectron imaging spectroscopic signatures of CO activation by the heterotrinuclear titanium-nickel clusters, *Chinese Chemical Letters* (2022), doi: https://doi.org/10.1016/j.cclet.2022.07.045

Photoelectron imaging spectroscopic signatures of CO activation by the heterotrinuclear titanium-nickel clusters

Jianpeng Yang [a,*], Jumei Zhang [b,c], Shihu Du [b], Gang Li [b], Jinghan Zou [b], Qiangshan Jing [a], Hua Xie [b,*], Ling Jiang[b,*]

[a]*College of Chemistry and Chemical Engineering, Xinyang Normal University, Xinyang 464000, China*
[b]*State Key Laboratory of Molecular Reaction Dynamics, Dalian Institute of Chemical Physics, Chinese Academy of Sciences, Dalian 116023, China*
[c]*School of Life Science, Ludong University, Yantai 264025, China.*

Graphical Abstract

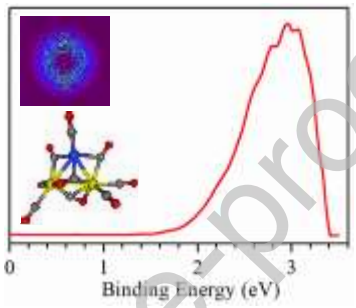

The CO activation by metal clusters plays an essential role in various areas, such as catalysis and organometallic synthesis. Photoelectron velocity-map imaging spectroscopy of heterotrinuclear $Ti_2Ni(CO)_n^-$ carbonyls reveals the capability of simultaneously accommodating the terminal, bridging, and side-on bonding modes, pointing to the weak, moderate, high C–O bond activation.

ARTICLE INFO

Article history:
Received 18 June 2022
Received in revised form 11 July 2022
Accepted 19 July 2022
Available online

Keywords:
CO activation
Transition metal carbonyl
Heteronuclear cluster
Photoelectron imaging
Quantum chemical calculations

ABSTRACT

A series of heterotrinuclear $Ti_2Ni(CO)_n^-$ (n = 6-9) carbonyls have been generated *via* a laser vaporization supersonic cluster source and characterized by mass-selected photoelectron velocity-map imaging spectroscopy. Quantum chemical calculations have been carried out to identify the structures and understand the experimental spectral features. The results indicate that a building block of Ti-Ti-Ni-C four-membered ring with the C atom bonded to Ti, Ti, and Ni is dominated in the n = 6-8 complexes, whereas a structural motif of Ti-Ti-Ni triangle core is preferred in n = 9. These complexes are found to be capable of simultaneously accommodating all the main modes of metal-CO coordination (*i.e.*, terminal, bridging, and side-on modes), where the corresponding mode points to the weak, moderate, high C–O bond activation, respectively. The number of CO ligands for a specific bonding mode varies with the cluster size. These findings have important implications for molecular-level understanding of the interaction of CO with alloy surfaces/interfaces and tuning the appropriate CO activation via the selection of different metals.

∗ Corresponding authors.
E-mail addresses: yangjpchem@126.com (J. Yang), xiehua@dicp.ac.cn (H. Xie), ljiang@dicp.ac.cn (L. Jiang).

Metal clusters may represent the low-coordinate sites on the surface and are often regarded as models for the surface of bulk materials [1]. The interactions of metal clusters with carbon monoxide (CO) play an essential role in various areas, such as heterogeneous and homogeneous catalysis, organometallic synthesis, and coordination chemistry [2-5]. The model systems of metal carbonyls can be studied under well-defined conditions to explore the multifaceted mechanisms of CO chemisorption on metal surfaces and the structure-reactivity relationships. Mononuclear metal carbonyls have been extensively explored by various experimental methods, such as collision-induced dissociation [6-8], infrared spectroscopy [9-15], microwave spectroscopy [16], and photoelectron spectroscopy [17-20]. Along with significant advances in theoretical calculations, the studies on the reactions of heterodinuclear transition metal clusters with CO have provided great insights into the nature of chemical bonding, the synergy effects of different transition metals on the catalytic performance, and different structural features [21-25].

The CO ligand generally coordinates with metals in terminal, bridging, and sided-on modes, in which the degree of CO activation is weak, moderate, and high, respectively. In the homodinuclear transition metal carbonyls $Ti_2(CO)_n^-$ (n = 3-9) [26], the CO ligands bind to Ti_2 in a side-on fashion and form a stable $Ti_2[\eta^2(\mu_2\text{-C, O})]_3$ structure at n = 3, the motif of which retains up to n = 5. With the increase of cluster size, one of side-on CO disappears, two side-on CO modes remain and the other CO is terminally bonded to Ti atom. In the heterodinuclear transition metal carbonyls $TMNi(CO)_n^-$ (TM = Ti, Zr, Hf; n = 3-7) [18], three different types of CO bonds (*i.e.*, terminal, bridging, and sided-on modes) are simultaneously formed at n = 3, whereas side-on CO mode disappears at n = 6. These results indicate that consecutive addition of CO ligands on the metal clusters would weaken the degree of CO activation. While early transition metal carbonyls exhibit rich fashion of different CO coordination modes, CO is terminally bonded to late transition metals in general, such as $AgFe(CO)_4$ [27], $CuFe(CO)_{4\text{-}7}$ [28], $CuNi(CO)_{2\text{-}4}$ [23], $FeCo(CO)_8$ [29], $FeZn(CO)_5$ and $CoZn(CO)_7$ [30]. Herein, we report a study on a series of heterotrinuclear $Ti_2Ni(CO)_n^-$ (n = 6-9) using photoelectron velocity-map imaging spectroscopy and quantum chemical calculations. A building block of Ti-Ti-Ni-C is favorably formed at n = 6 to produce an irregular four-membered ring with the C atom bonded to Ti, Ti and Ni, the structure of which persists up to n = 8. A Ti-Ti-Ni triangle core structure is dominated at n = 9.

The experiments were performed using a homemade dual-channel time-of-flight mass spectrometer (D-TOFMS) coupled with velocity-map photoelectron imaging analyzer [31]. The $Ti_2Ni(CO)_n^-$ (n = 6-9) complexes were prepared by laser vaporization of Ti-Ni alloy in a supersonic expansion of 5% CO/helium (see Supporting information for experimental details). The photoelectron images and the corresponding photoelectron spectra (PES) of $Ti_2Ni(CO)_n^-$ (n = 6-9) at 355 nm (3.496 eV) are shown in Fig. 1. The dominant main peak labeled with the letter X in each spectrum, has a distinct band maximum, which directly determines the ground-state vertical detachment energy (VDE) values. While the adiabatic detachment energies (ADEs) of the ground state transition are roughly estimated by extrapolating the lower electron binding energy (EBE) side of the band to the binding energy axis and then adding the instrumental resolution to the intersection with the binding energy axis. The measured VDEs and ADEs are listed in Table 1.

Table 1. Comparison of experimental VDE and ADE values to BP86 calculated ones of the five lowest-energy isomers for $Ti_2Ni(CO)_n^-$ (n = 6-9).

Cluster	Isomer	Relative energy (eV)	VDE (eV)		ADE (eV)	
			Expt.[a]	Calcd.	Expt.[a]	Calcd.
n = 6	6A	0.00	2.45(5)	2.52	2.05(7)	2.11
	6B	0.16		3.01		2.78
	6C	0.58		2.69		2.30
	6D	0.80		2.48		2.27
	6E	0.98		2.75		2.64
n = 7	7A	0.00	2.62(4)	2.63	2.10(7)	2.26
	7B	0.07		2.99		2.54
	7C	0.12		2.80		2.50
	7D	0.50		3.05		2.83
	7E	0.63		2.62		1.99
n = 8	8A	0.00	2.65(4)	2.70	2.14(7)	2.33
	8B	0.11		3.24		2.84
	8C	0.17		2.93		2.79
	8D	0.36		3.00		2.78
	8E	0.60		2.82		2.51
n = 9	9A	0.00	3.02(2)	3.13	2.50(5)	2.77
	9B	0.13		3.45		3.01
	9C	0.23		3.05		2.91
	9D	0.25		2.73		2.56
	9E	0.51		3.15		2.81

[a]Numbers in parentheses represent the uncertainty in the last digit.

As shown in Fig. 1, the PES spectrum of $Ti_2Ni(CO)_6^-$ is split into two apparent bands where the lower energy band centered at 2.45 eV (labeled with X) is considered as the ground-state VDE and the higher energy band centered at 3.05 eV may be attributed to the isomer with a relatively higher energy, in which the intensity of the former band is slightly larger than that of the latter band. The spectrum of $Ti_2Ni(CO)_7^-$ is the widest one among the four species with an onset at around at 2.0 eV, indicating that several nearly

isoenergetic isomers might be present. The spectrum of $Ti_2Ni(CO)_8^-$ appears as two bands with the lower energy band centered at around 2.65 eV and the higher energy band centered at 3.0 eV. Contrary to n = 6, the higher energy band is more intense than the lower energy band at n = 8. While for $Ti_2Ni(CO)_9^-$, the spectrum contains only one band centered at 3.02 eV.

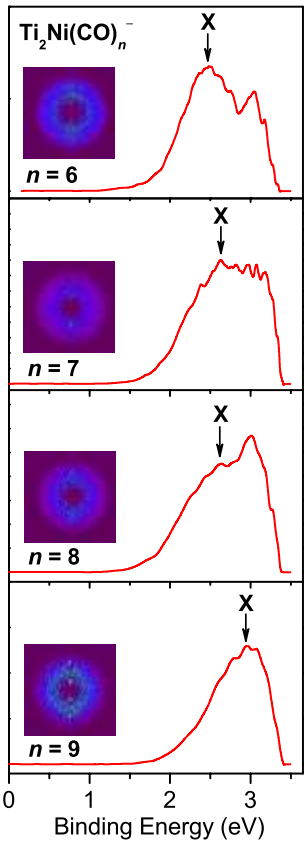

Fig. 1. Photoelectron spectra of $Ti_2Ni(CO)_n^-$ (n = 6-9) recorded at 355 nm (3.496 eV). Photoelectron images after inverse Abel transformation are embedded in the photoelectron spectra.

To understand the experimentally observed spectral features and identify the structures of the $Ti_2Ni(CO)_n^-$ complexes, quantum chemical calculations were carried out at the BP86/def2-TZVP level of theory (see Supporting information for theoretical details). The optimized structures of the five lowest-lying isomers for $Ti_2Ni(CO)_n^-$ (n = 6-9) are illustrated in Fig. 2. The calculated values of VDEs and ADEs are compared with the experimental ones in Table 1.

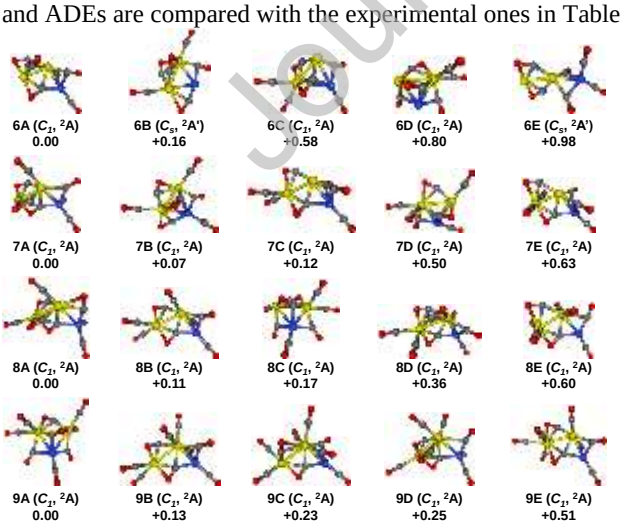

Fig. 2. Optimized structures of the five lowest-energy isomers for $Ti_2Ni(CO)_n^-$ (n = 6-9) (Ti, yellow; Ni, blue; C, gray; O, red). Relative energies are given in eV.

The most stable isomer of $Ti_2Ni(CO)_6^-$, labeled as 6A, has a C_1 structure with a ^{2}A ground state (Fig. 2), forming an irregular four-membered ring of Ti-Ti-Ni-C unit. The 6A isomer contains two side-on COs, three bridging COs, and one terminal CO. The calculated

VDE and ADE of 6A is 2.52 and 2.11 eV (Table 1), respectively, consistent with the corresponding experimental value of the lower energy band (2.45 and 2.05 eV). The 6B isomer is 0.16 eV higher in energy than 6A, which includes three side-on carbonyls, one carbonyl terminally bonded to the Ti atom, one carbonyl terminally bonded to another Ti atom, one bridging carbonyl bonded to the Ti and Ni atoms. The calculated VDE and ADE of 6B is 3.01 and 2.78 eV (Table 1), respectively, which agree well with the corresponding experimental value of the higher energy band (3.05 and 2.84 eV). The 6C isomer lies 0.58 eV higher than 6A. 6C includes a Ti-Ti-Ni triangle core, one side-on carbonyl bonded to the triangle core, one side-on carbonyl bonded to Ti-Ti, one bridging carbonyl bonded to Ti and Ni atoms, two carbonyls terminally bonded to Ti atom, one carbonyl terminally bonded to Ni atom. The calculated VDE and ADE of 6C is 2.69, 2.30 eV, respectively, which are much larger than the experimental values of the lower energy band and remarkably smaller than those of the higher energy band. The 6D isomer lies 0.80 eV higher than 6A, which includes a Ti-Ti-Ni triangle core, a side-on carbonyl bonded to triangle core, a side-on carbonyl bonded to Ti-Ti, two bridging carbonyls bonded to Ti-Ni, two carbonyls terminally bonded to Ti atom. The 6E is 0.98 eV higher than 6A, which includes two side-on carbonyls bonded to Ti-Ti, two bridging carbonyls bonded to Ti-Ni, two carbonyls terminally bonded to Ni atom. The isomers 6D and 6E should be too high in energy to be probed in the experiment. Thus, the 6A and 6B isomers are responsible for the $Ti_2Ni(CO)_6^-$ spectrum.

The most stable isomer of $Ti_2Ni(CO)_7^-$ (7A) consists of a C_1 structure with a ^2A ground state. The 7A isomer holds a similar structural characteristic of four-membered ring of 6A and consists of three side-on carbonyls, one bridging carbonyl, and three terminal carbonyls. The calculated VDE and ADE of 7A is 2.63 and 2.26 eV (Table 1), respectively, which are in accord with the experimental results (2.62 and 2.10 eV). The 7B isomer lies above 7A by 0.07 eV, which includes a Ti-Ti-Ni triangle core, three side-on carbonyls, one bridging carbonyl, and three terminal carbonyls. The predicted VDE and ADE values of 7B (2.99 and 2.54 eV) fall in the region of the broad experimental band (Fig. 1). The 7C isomer lies 0.12 eV higher than 7A, which includes two side-on carbonyls, two bridging carbonyls, and three terminal carbonyls. The calculated VDE and ADE values (2.80 and 2.50 eV) also agree with the broad experimental band. The 7D isomer is 0.50 eV higher than 7A, which includes a Ti-Ti-Ni triangle core, two side-on carbonyls bonded to Ti-Ti, one bridging carbonyl bonded to Ti-Ni, and four terminal carbonyls. The 7E isomer is 0.63 eV higher than the most stable isomer and includes two side-on carbonyls, two bridging carbonyls and three terminal carbonyls. Given that the relative energies of 7D and 7E are much higher than 7A, these two isomers might not contribute to the $Ti_2Ni(CO)_7^-$ spectrum. The agreement between theory and experiment indicates the co-existence of the 7A, 7B and 7C isomers.

The most stable isomer of $Ti_2Ni(CO)_8^-$ (8A) has four side-on carbonyls and four terminal carbonyls. The building block of Ti-Ti-Ni-C four-membered ring still exists in 8A. The theoretical VDE and ADE value is 2.70 and 2.33 eV (Table 1), respectively, which reproduce well the experimental results (2.65 and 2.14 eV). The 8B isomer is 0.11 eV higher than 8A, which includes two side-on carbonyls, two bridging carbonyls, and four terminal carbonyls. The computed VDE and ADE value of 8B is 3.24, 2.84 eV, respectively, which are much larger than the higher energy band. The 8C isomer is 0.17 eV higher than 8A, which includes three side-on carbonyls, two bridging carbonyls, and three terminal carbonyls. The theoretical VDE and ADE of 8C is 2.93 and 2.79 eV, respectively, which is in accordance with the corresponding experimental value of the higher energy band (3.00 and 2.85 eV). The 8D isomer is 0.36 eV higher than 8A, which includes three side-on carbonyls, two bridging carbonyls, and three terminal carbonyls. Even though the theoretical VDE and ADE values (3.00 and 2.78 eV) are close to the experimental values of the higher energy bond, the simulated photoelectron spectrum of 8D is quite different from the experimental spectrum (Fig. S2 in Supporting information). The 8D isomer could be ruled out. The 8E isomer lies 0.60 eV above 8A, which includes two side-on carbonyls, one bridging carbonyl and five terminal carbonyls. The 8E isomer could be too high in energy to be probed in the experiment. Therefore, the 8A and 8C isomers should be responsible for the $Ti_2Ni(CO)_8^-$ spectrum.

In the most stable isomer of $Ti_2Ni(CO)_9^-$ (9A), a Ti-Ti-Ni triangle core is formed. The 9A structure includes two side-on carbonyls, two bridging carbonyls, and five terminal carbonyls. The theoretical VDE and ADE value is 3.13 and 2.77 eV (Table 1), respectively, which match with the experimental values (3.02 and 2.50 eV). The 9B isomer lies 0.13 eV higher than 9A, which includes two side-on carbonyls, two bridging carbonyls, and five terminal carbonyls. The computed VDE and ADE value is 3.45 and 3.01 eV, respectively, which are noticeably higher than the experimental values. The 9C isomer is 0.23 eV higher than 9A, which includes two side-on carbonyls, two bridging carbonyls, and five terminal carbonyls. The theoretical VDE and ADE value of 9C is 3.05 and 2.91 eV, respectively, which are also higher than the experimental values. The 9D isomer is 0.25 eV higher than 9A, which includes three side-on carbonyls, one bridging carbonyl, and five terminal carbonyls. The theoretical VDE value of 9D (2.73 eV) is much lower that the experimental value (3.02 eV), even though its theoretical ADE value (2.56 eV) is close to the experimental value (2.56 eV). The 9E isomer is 0.51 eV higher than 9A, which includes two side-on carbonyls, one bridging carbonyl, and six terminal carbonyls. The theoretical VDE and ADE of 9E is 3.15 and 2.81 eV, respectively. However, the relative energy of 9E is too high to exist in the experiment. It can be concluded that the calculated results of 9A agree best with the experimental ones and 9A should be responsible for the $Ti_2Ni(CO)_9^-$ spectrum.

The agreement of the calculated results with experiment is reasonable to establish the structural evolution of $Ti_2Ni(CO)_n^-$ (n = 6-9). The spectra of all cluster sizes, especially for n = 6-8, show a high energy band around 3.0 eV, suggesting that both the Ti-Ti-Ni-C four-membered ring and the Ti-Ti-Ni triangle core might co-exist in n = 6-8. The intensity of this higher energy band increases with the increase of cluster size, indicating that the triangle core becomes more favorable in the larger clusters. The VDE value of the most stable structure for n = 6-8 increases with the increasing cluster size, indicating that the sequential bonding of the CO molecules stabilizes the negative electron.

The C-O bond lengths of side-on, bridging, and terminal carbonyls in the lowest-energy isomers for $Ti_2Ni(CO)_n^-$ (n = 6-9) are shown in Fig. 3. The bond length of the side-on CO ligand bonded to the Ti-Ti-Ni unit in the 6A-9A isomers is calculated to be 1.29, 1.28,

1.26, and 1.23 Å, respectively, evidencing a monotonical shortening with the increase of cluster size. The stretching frequency of these side-on CO is predicted to be 1327, 1358, 1422, and 1550 cm^{-1} (Table S1 in Supporting information), respectively, supporting the trend of C-O bond lengths. The bond length of the side-on C-O bonded to Ti-Ti is calculated to be 1.27, 1.29, 1.25 and 1.23 Å, respectively, and the corresponding CO stretching frequency is predicted to be 1360, 1309, 1448 and 1559 cm^{-1} (Table S1). These stretching frequencies of the side-on CO ligands are remarkably redshifted from that of the free CO molecule (2121 cm^{-1} calculated at the same theory level), indicating these C-O bonds are significantly weakened. In the isomers consisting of bridging CO bonded to the Ti-Ni unit (6A, 7A and 9A), the C-O bond lengths are calculated to be about 1.18 Å (Fig. 3) with the corresponding CO stretching frequencies around ~1780 cm^{-1} (Table S1). The bond length of the terminal CO bonded to the Ni atom in the 6A-9A isomers is calculated to be 1.17, 1.16, 1.16 and 1.16 Å, respectively, with the corresponding CO stretching frequencies predicted at 1941, 1933, 1973, and 1984 cm^{-1} (Table S1).

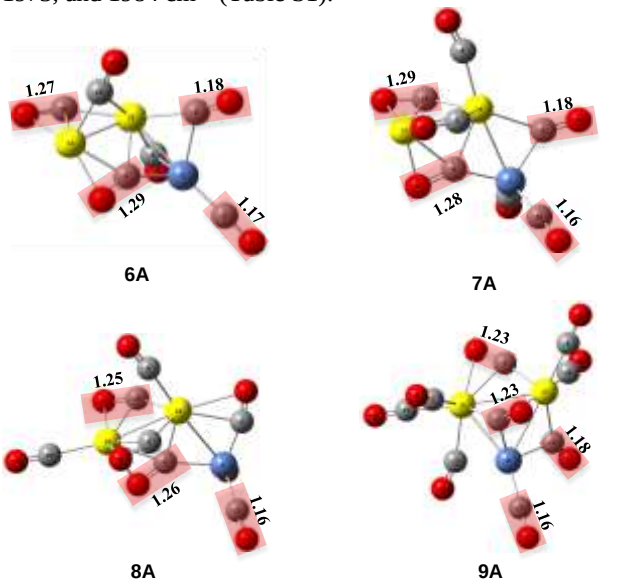

Fig. 3. The C-O bond lengths (in angstrom) of side-on, bridging, and terminal carbonyls in the most stable isomers (6A-9A) for $Ti_2Ni(CO)_n^-$ (n = 6-9) (Ti, yellow; Ni, blue; C, gray; O, red) calculated at the BP86/def2-TZVP level of theory.

It can be seen from Fig. 3 that the bond length of the side-on CO bonded to Ti-Ti-Ni is similar to that of the side-on CO bonded to Ti-Ti (1.23~1.29 Å), which are much longer than that of the free CO molecule (1.13 Å). The bond lengths of side-on COs are also longer than those of bridging COs and terminal COs, indicating that the activation degree of these side-on COs is stronger than that of bridging CO and terminal CO.

To elucidate the electronic structures of $Ti_2Ni(CO)_n^-$ (n = 6-9), the highest occupied molecular orbitals (HOMO) of the most stable isomers of $Ti_2Ni(CO)_n^-$ (n = 6-9) down to the fourth valence orbital from the HOMO are shown in Fig. 4. The HOMO, HOMO-1 and HOMO-2 of isomer 6A feature π-type bonds with striking metal to carbonyl donations. The HOMO-3 and HOMO-4 of 6A are mainly delocalized π orbitals, in which metal-metal interaction is mainly involved. Analogous chemical bonding features are also observed in the 7A-9A isomers.

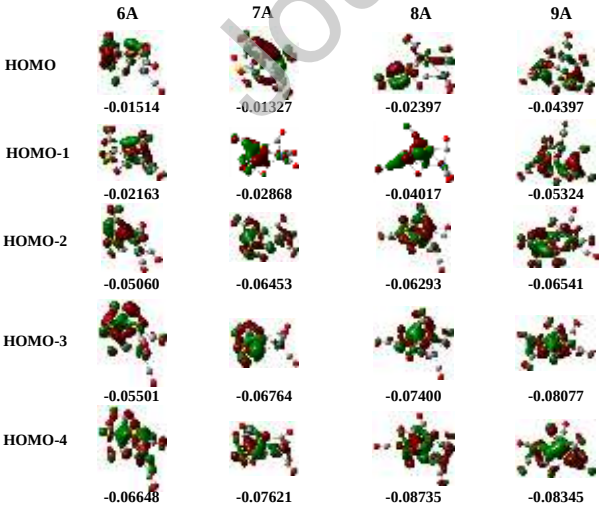

Fig. 4. Molecular orbital pictures of the most stable isomers for $Ti_2Ni(CO)_n^-$ (n = 6-9) (6A-9A), showing the highest occupied molecular orbitals (HOMO) down to the fourth valence molecular orbital from the HOMO (Isovalue = 0.04). The orbital energies are given in hartree.

The terminal and bridging bonding modes of CO on the metal catalysts are common features as well known. The unusual C-O bond weakening was also observed for chemisorbed CO in side-on modes on some transition metal surfaces, where the CO stretching frequencies appeared in the 1100-1400 cm^{-1} region [10,32-35]. It can be inferred from the above analysis that all the terminal, bridging, and side-on bonding modes of CO are involved in these $Ti_2Ni(CO)_n^-$ complexes, corresponding to the weak, moderate, high C–O bond activation, respectively. These results would advance our fundamental understanding of the structure and bonding mechanism of CO activation and chemisorbed CO molecules on heteronuclear metal clusters and surfaces.

In summary, mass-selected photoelectron velocity-map imaging spectroscopic and quantum chemical studies of $Ti_2Ni(CO)_n^-$ (n = 6-9) have been carried out to elucidate the geometric and electronic structures of hetero-polynuclear carbonyls. For n = 6-8, both the Ti-Ti-Ni-C four-membered ring and Ti-Ti-Ni triangle core co-exist in the experimental spectra with the former structure contributing to the lower energy band and the latter structure contributing to the higher energy bond. While for n = 9, the higher energy band dominates the spectrum, implying a main contribution of the Ti-Ti-Ni triangle motif. The C–O bonds are apparently weakened in these $Ti_2Ni(CO)_n^-$ (n = 6-9) complexes. The present findings provide important insights into the structure and bonding mechanisms of the interaction of CO molecules with heteronuclear metals and unravel mechanical understanding of CO activation on alloy surfaces at the molecular level.

Acknowledgment

The authors gratefully acknowledge the Dalian Coherent Light Source (DCLS) for support and assistance. This work was supported by the National Natural Science Foundation of China (Nos. 21873097, 22103082, 92061203, 22125303 and 22288201), the Youth Innovation Promotion Association of the Chinese Academy of Sciences (CAS, No. 2020187), and the Strategic Priority Research Program of CAS (No. XDB17000000).

References

[1] B. Yoon, H. Hakkinen, U. Landman, et al., Science 307 (2005) 403-407.

[2] A.W. Castleman, R.G. Keesee, Acc. Chem. Res. 19 (1986) 413-419.

[3] D.K. Bohme, H. Schwarz, Angew. Chem. Int. Ed. 44 (2005) 2336-2354.

[4] S.M. Lang, T.M. Bernhardt, Phys. Chem. Chem. Phys. 14 (2012) 9255-9269.

[5] H.J. Freund, G. Meijer, M. Scheffler, et al., Angew. Chem. Int. Ed. 50 (2011) 10064-10094.

[6] L.S. Sunderlin, D.N. Wang, R.R. Squires, J. Am. Chem. Soc. 114 (1992) 2788-2796.

[7] X.G. Zhang, P.B. Armentrout, Organometallics 20 (2001) 4266-4273.

[8] F. Meyer, Y.M. Chen, P.B. Armentrout, J. Am. Chem. Soc. 117 (1995) 4071-4081.

[9] M.F. Zhou, L. Andrews, J. Phys. Chem. A 103 (1999) 6956-6968.

[10] I. Swart, F.M.F. de Groot, B.M. Weckhuysen, et al., J. Am. Chem. Soc. 130 (2008) 2126-2127.

[11] A.D. Brathwaite, Z.D. Reed, M.A. Duncan, J. Phys. Chem. A 115 (2011) 10461-10469.

[12] A.M. Ricks, Z.E. Reed, M.A. Duncan, J. Mol. Spectrosc. 266 (2011) 63-74.

[13] A.D. Brathwaite, M.A. Duncan, J. Phys. Chem. A 117 (2013) 11695-11703.

[14] P. Ferrari, J. Vanbuel, T. Nguyen Minh, et al., Chem. Eur. J. 23 (2017) 4120-4127.

[15] H.A. Abdulhussein, P. Ferrari, J. Vanbuel, et al., Nanoscale 11 (2019) 16130-16141.

[16] T. Okabayashi, T. Yamamoto, E.Y. Okabayashi, M. Tanimoto, J. Phys. Chem. A 115 (2011) 1869-1877.

[17] J.E. Reutt, L.S. Wang, Y.T. Lee, D.A. Shirley, Chem. Phys. Lett. 126 (1986) 399-404.

[18] J. Zou, H. Xie, Q. Yuan, et al., Phys. Chem. Chem. Phys. 19 (2017) 9790-9797.

[19] H. Xie, J. Zou, Q. Yuan, et al., Top. Catal. 61 (2018) 71-80.

[20] G. Li, J. Zhang, H. Xie, et al., J. Phys. Chem. A 122 (2018) 3811-3818.

[21] H. Schwarz, Angew. Chem. Int. Ed. 54 (2015) 10090-10100.

[22] G. Wang, M. Zhou, Chin. J. Chem. Phys. 31 (2018) 1-11.

[23] Z. Liu, H. Xie, Z. Qin, et al., Inorg. Chem. 53 (2014) 10909-10916.

[24] J. Zhang, G. Li, Q. Yuan, et al., J. Phys. Chem. A 124 (2020) 2264-2269.

[25] J. Zhang, Y. Li, Y. Bai, et al., Chin. Chem. Lett. 32 (2021) 854-860.

[26] J. Zou, H. Xie, D. Dai, et al., J. Chem. Phys. 145 (2016) 184302.

[27] Z. Liu, Y. Bai, Y. Li, et al., Dalton Trans. 49 (2020) 15256-15266.

[28] N. Zhang, M. Luo, C. Chi, et al., J. Phys. Chem. A 119 (2015) 4142-4150.

[29] H. Qu, F. Kong, G. Wang, M. Zhou, J. Phys. Chem. A 120 (2016) 7287-7293.

[30] H. Qu, F. Kong, G. Wang, M. Zhou, J. Phys. Chem. A 121 (2017) 1628-1633.

[31] Z. Qin, X. Wu, Z. Tang, Rev. Sci. Instrum. 84 (2013) 066108.

[32] F.M. Hoffmann, R.A. Depaola, Phys. Rev. Lett. 52 (1984) 1697-1700.

[33] L. Jiang, Q. Xu, J. Am. Chem. Soc. 127 (2005) 42-43.

[34] H.J. Zhai, B. Kiran, B. Dai, et al., J. Am. Chem. Soc. 127 (2005) 12098-12106.

[35] C. Chi, H. Qu, L. Meng, et al., Angew. Chem. Int. Ed. 56 (2017) 14096-14101.